NOVEL ELECTROSTATIC REPULSION FORCES IN MEMS APPLICATIONS BY NONVOLATILE CHARGE INJECTION

Zengtao Liu, Myongseob Kim, Nick Shen and Edwin C. Kan
School of Electrical and Computer Engineering, Cornell University, Ithaca, NY 14853

ABSTRACT

This paper demonstrates, for the first time, electrostatic repulsion forces between two isolating beams as a viable actuation mechanism in MEMS applications by nonvolatile charge injection. Devices integrating MEMS beams and EEPROM structures have been fabricated and actuation force of ~0. 2μN has been recorded across a 3μm gap for beams 360μm in length. Larger actuation forces can be achieved through smaller gaps. A capacitor-network model is presented for analyzing such systems. This scheme holds promises in complimenting attractive electrostatic actuation and also finds valuable applications in achieving wear-free micro-bearings, hinges and turbines.

INTRODUCTION

Electrostatic actuators have been used extensively in MEMS applications for their simplicities in fabrication and operation [1]. However, the conventional electrostatic actuation scheme through attractive forces faces a few limitations, including limited travel distance, highly nonlinear voltage-position relationships, and inability to tune the resonant frequency, etc [2]. These limitations can potentially be addressed by the introduction of electrostatic repulsion forces. However, electrostatic repulsion as an actuation scheme requires efficient manipulation of static charges with the same polarity in a controllable fashion and has not yet been demonstrated.

Electrostatic repulsion forces have been observed in lateral comb drives as the cause of their levitation [3]. It is also postulated as the mechanism for micro-hinge assembly using ultrasonic triboelectricity [4]. Neither approach can serve as an effective actuation method. In the former case, charges are generated through electrostatic coupling which is difficult to control because of the high voltage and complex structures required for efficient deployment. The second one is caused by direct charge injection that poses limitations on integration and packaging, as exposure to charging sources is necessary.

In this paper we propose using nonvolatile charge injection to realize effective electrostatic repulsion force actuation. As shown in Fig. 1, MEMS structures are integrated with Electrically Erasable Programmable Read Only Memory (EEPROM) cells [5] and are electrically connected with the floating gate of the EEPROMs. Nonvolatile charges can be added and removed from the floating gate through hot-electron injection or F-N tunneling, and monitored by the threshold voltage shift in EEPROM. This approach simplifies the design and integration, enables dynamic control during operation, and has the potential to achieve low-voltage operations. It can be used either as a stand-alone actuation scheme or in compliment with the conventional electrostatic actuation for improvement of linearity, travel distance or tuning of effective mass, resonant frequency, and harmonic response.

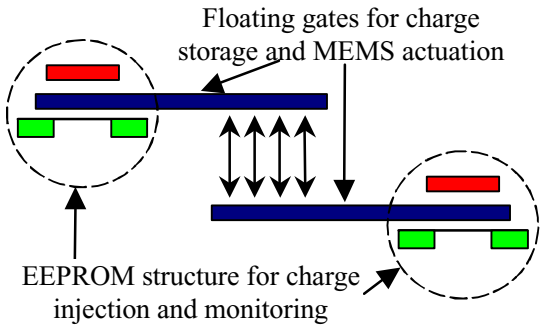

Figure 1. Schematic diagram for electrostatic repulsion force actuation through integration of MEMS and EEPROM structures.

EXPERIMENTAL SETUP

We seek the proof of concept using foundry service (AMI 1.5μm technology with double poly) provided by MOSIS [6] combined with post processing. The advantage of this approach is that we can have a controlled CMOS process with good CMOS and EEPROM characteristics. The disadvantage is that we do not have control over the processing conditions and have to take the small inter-layer spacing and built-in compressive stress in the poly-silicon films inherent to standard CMOS technology. To overcome these limitations and ensure proper MEMS operation, a post processing technique consisting of Si substrate undercut and selective oxide release is developed and special attention is paid during the layout design.

In the layout, EEPROM devices are spatially separated from the MEMS components by a minimum clearance of 50μm. This way a MEMS release window can be defined during the post processing with the EEPROM devices protected. Extensive oxide openings are also placed within the MEMS release window to undercut the Si substrate below movable structures for increased vertical spacing. Fig. 2 illustrates the post processing sequence.

0-7803-7185-2/02/$10.00 ©2002 IEEE

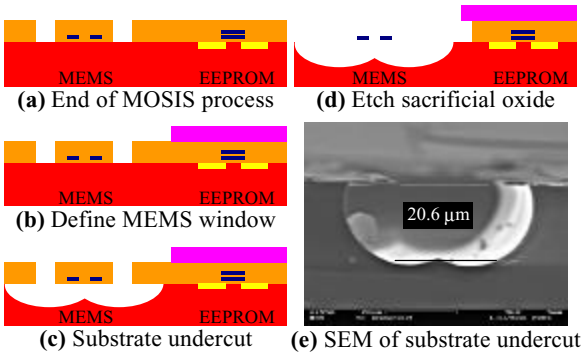

Figure 2. Post processing sequence and a SEM image showing the substrate undercut.

From the MOSIS chip, one more lithograph step defines the MEMS release window and ~5µm photo resist is left on top of the EEPROM devices as a protection layer throughout the post processing. Then the Si substrate below MEMS devices is undercut by isotropic etching in SF_6 plasma through the oxide openings created in MOSIS process. A cross section of the substrate undercut is also shown in Fig. 2. This step is critical in order to generate enough spacing for vertical travel and avoid stiction. It also helps to improve the release yield and efficiency during the etching of sacrificial oxide because it allows the etchant to attack oxide from underneath. The MEMS devices are released in the 777 etchant (Acetic acid + Ammonium fluoride + water) and dried by supercritical CO_2. The release time has to be accurately controlled to protect the EEPROM and interconnect integrity. The 777 etchant is selected over HF because it attacks aluminum slower, which is used for interconnects and some of them may be exposed during the release.

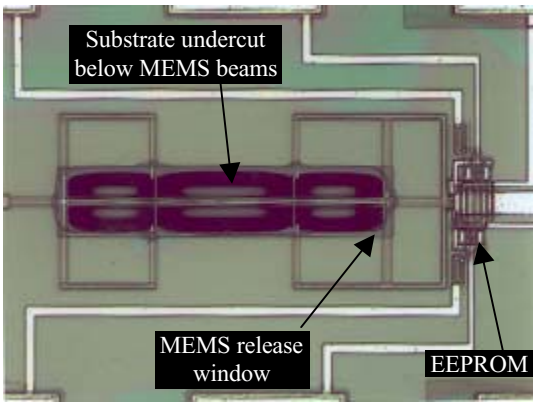

Figure 3. Micrograph of a released device for electrostatic repulsion force demonstration.

MEASUREMENT RESULTS

The devices for electrostatic repulsion force demonstration consist of pairs of parallel beams of various lengths (160 ~ 400µm) with 1.6µm (design rule minimum) gap. The beams are anchored at both ends by oxide. Each beam connects to the floating gate of an EEPROM cell for charge injection and monitoring. When nonvolatile charges of the same polarity are injected into the beams, the electrostatic repulsion forces generated between them will deflect the beams and it can be observed under microscope. A released device with 360µm beams is shown in Fig. 3.

Due to the large capacitance of the MEMS beams, when a large positive bias is applied on the control gate of the EEPROMs, F-N tunneling occurs between the floating and control gate. As the result, electrons are extracted from the floating gate and cause a negative threshold voltage shift. It has been demonstrated that $|\delta V_{TH}|$ greater than 10V can be achieved, which corresponds to ~3pC charges on the floating gate for our devices. The typical EEPROM I-V characteristic is shown in Fig. 4.

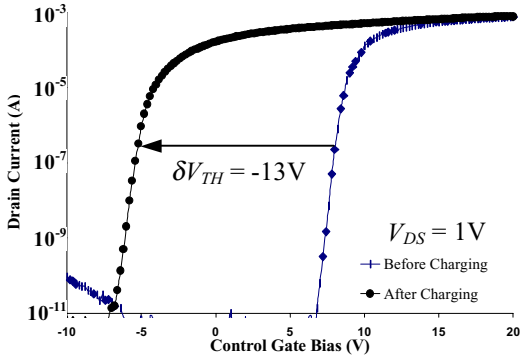

Figure 4. Typical I-V characteristics of the EEPROM devices before and after charge injection. Charge injection is done by F-N tunneling at 45V control gate bias.

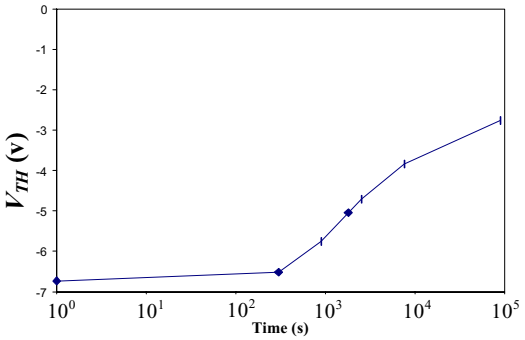

Figure 5. Device charge retention characteristics.

For long-term nonvolatile operations, the floating gates have to be able to retain the injected charges. Fig. 5 shows the charge retention characteristics of a released device. Charges can be retained for days but significant degradation starts to occur only a few minutes after injection. This is mainly due to the fixed MOSIS process. Because of the small interlayer spacing and built-in compressive stress, inadvertent contact to the substrate can be easily generated at the edge of the MEMS release window, which draws excessive leakage current from the floating gate and reduce the retention time. Direct air exposure of the MEMS beams also poses great challenge for achieving long retention time. These drawbacks can be alleviated by better design or a custom technology with more ideal anchors and insulator-coated beams.

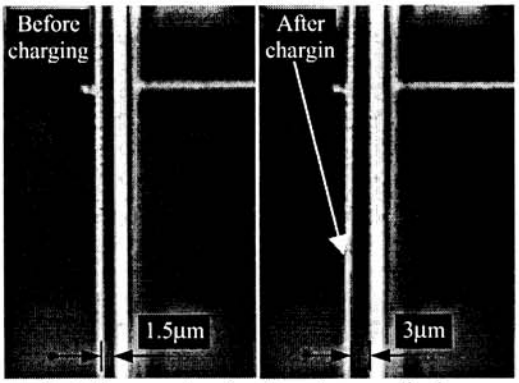

Figure 6. Micrograph showing beam displacement by electrostatic repulsion force after nonvolatile charge injection.

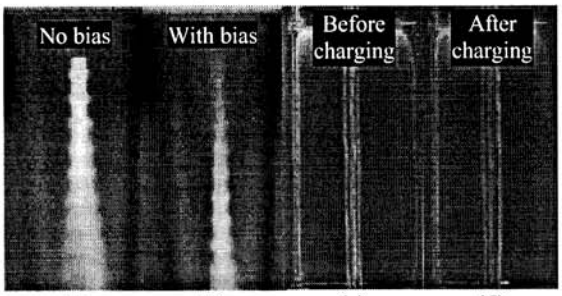

Figure 7. Electrostatic forces caused by (a)(b): voltage coupling and (c)(d): direct electron charging under SEM.

Fig. 6 shows the displacement of a MEMS beam by electrostatic repulsion force after nonvolatile charge injection. The beams are 360μm long and made of poly-silicon of 0.3μm thick. The center and side beams are 2.4μm and 1.6μm wide, respectively. While all three beams are charged simultaneously, only the left beam is deflected after charging because the right beam is also anchored in the middle by the sidebars while the center beam experiences rather balanced forces from both sides. Charging is performed through F-N tunneling by biasing the control gate of the corresponding EEPROM cells at 45V for 10 seconds. Threshold voltage shift of ~15V is observed after charging. Beam displacement of ~1.5μm at the mid point can be clearly observed from Fig. 6. Assuming uniform force distribution along the beam, the electrostatic repulsion force required to generate the amount of deflection is calculated to be ~0.21μN based on the Young's modulus of poly-silicon.

For comparison purposes, we also demonstrated electrostatic repulsion forces through voltage coupling and direct electron injection. In Fig. 7 (a) and (b), another two electrodes (cannot be seen) are hanging over the beam. When a large voltage is applied to those electrodes and the beam simultaneously, the induced charges in them are of the same polarity and deflect the beam out of focus. In (c) and (d), beam deflection of ~2μm is observed after charging by electron bombardment in a SEM.

ANALYSIS AND DISCUSSIONS

Exact calculation of the electrostatic repulsion force for devices shown in Figs. 3 and 6 is very difficult because the beam deformation and the charge distribution are both non-uniform and interfere with each other. However, the total charges in the beams can be estimated by the capacitor network model shown in Fig. 8 rather straightforwardly. Then by assuming uniform charge distribution along the beam, we can use this model to calculate the repulsion force to the first order and compare it with the experiments.

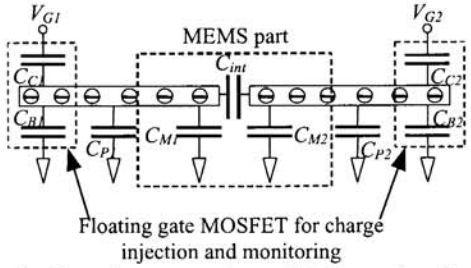

Figure 8. Capacitor network model for estimation of the nonvolatile charges injected into the MEMS beams.

Table 1. Components of the capacitor network

C_{C1} (C_{C2})	Capacitance between the floating gate 1(2) and control gate 1(2)
C_{B1} (C_{B2})	Capacitance between the floating gate 1(2) and Si substrate
C_{M1} (C_{M2})	Self-capacitance of MEMS beam 1(2)
C_{P1} (C_{P2})	Parasitic capacitance of MEMS beam 1(2)
C_{int}	Capacitance between the two MEMS beams

The meanings of the capacitor components in Fig. 8 are listed in Table 1. While C_C and C_B are necessary for charge injection, only charges stored in C_M are effective in generating the repulsion forces for actuation. C_{int} is also a very important design parameter. Larger C_{int} indicate stronger coupling between the two beams, which means larger repulsion force can be achieved with the same amount of charge, i.e. higher efficiency. However, this is only true for "common mode" operations. If there is a potential difference between the two beams, charges associated with C_{int} are of opposite polarity and attract each other, thus reducing the repulsion forces. This effect is proportional to C_{int} and poses stringent requirement on potential control for effective actuation. Therefore tradeoffs have to be made between the efficiency and controllability when designing C_{int}.

From the operation principles of EEPROMs, the total nonvolatile charges on the floating gate can be readily expressed as

$$Q_{1,2} = -C_{C1,2}\delta V_{TH} \qquad (1)$$

where δV_{TH} is the threshold voltage shift of the EEPROM cell. Assuming "common mode" and floating control gates during operation, charges on the floating gate will be divided among C_M, C_P and C_B with

$$Q_{M1,2} = -\frac{C_{C1,2}C_{M1,2}\delta V_{TH}}{C_{M1,2}+C_{P2,3}+C_{B1,2}} \qquad (2)$$

The above equations can serve as the design guidelines for systems employing the proposed actuation scheme. From them we can see that to generate large Q_M for effective actuation, large C_C and C_M are preferred. Moreover, if $C_M >> C_P+C_B$, Q_M will reduce to $C_C\delta V_{TH}$, which implies that all the injected charges are held by C_M.

To estimate the repulsion force demonstrated in Fig. 6 using this model, we have to first get the capacitance value for all the capacitors in Fig. 8. While C_C, C_B and C_P+C_M can be determined from the subthreshold swing of the EEPROMs, C_M has to be estimated from the device geometry. The results are listed in Table 2, together with the charges calculated using Equation 2.

Table 2. Estimated capacitance value for device in Fig. 6

Beam	C_C	C_B	C_P+C_M	C_M	Q_M
Left	253 fF	30 fF	315 fF	~11 fF	~0.12 pC
Center	253 fF	30 fF	286 fF	~14 fF	~0.16 pC
Right	253 fF	30 fF	315 fF	~11 fF	~0.12 pC

Neglecting beam deformation, the repulsion force between two uniformly charged beams can be calculated through line charge approximation as

$$F = \frac{Q_{M1}Q_{M2}}{2\pi\varepsilon_0 Ld} \qquad (3)$$

where L is the beam length and d is the distance between the two charge lines. Using data in Table 2 and average d of 4.8μm and 9.6μm for left-center and left-right beam interaction, respectively, the total repulsion force exerted on the left beam can be calculated by Equation 3 as ~0.28μN. This is in good agreement with the results from poly-silicon Young's modulus (~0.21μN), given the fact that both of them are rough estimations based on the assumptions of uniform charge and force distribution. For accurate force calculation, the charge distribution has to be determined by solving the 3D Poisson equation.

The demonstrated repulsion force is rather small in comparison with the forces required for most actuators. However, noticing the fact that C_M is more than one order of magnitude smaller than C_P, which implies very low efficiencies, we believe that forces in 1 ~ 10μN range can be achieved through design and process improvement.

FUTURE APPLICATIONS

Electrostatic repulsion force actuation can potentially change many MEMS device designs such as DMD and microwave switches. Since actuation happens at the short end of the travel range, it can significantly reduce the actuation voltage and increase the travel range. By introducing electrostatic repulsion forces locally in MEMS resonators by nonvolatile charge injection, it also helps in tuning its resonant frequency and harmonic response.

More interestingly, similar to the bullet train, the repulsion force can be used to eliminate physical contact and achieve *wear-free* micro-bearing, hinges and turbines, whose reliability is limited presently due to friction [7]. Electromagnetic friction can still exist due to charge flowing in structures with finite resistance. To further eliminate EM friction, the nonvolatile charges need to be confined in nanocrystals [8].

CONCLUSIONS

We have demonstrated electrostatic repulsion forces as a viable actuation mechanism in MEMS applications through nonvolatile charge injection. A capacitor network model is also presented for analyzing systems using such actuation scheme. Though the demonstrated force is smaller than required for effective actuation in most systems, larger forces can be obtained through design and process improvement, thus enable many novel applications.

ACKNOWLEDGEMENT

Part of the device fabrication was done at Cornell Nanofabrication Facilities (CNF). The authors would like to express their great appreciation to all the CNF staff for their kind help and support.

REFERENCES

[1] R. S. Muller, "Microdynamics," *Sensors and Actuators*, vol. A21-A23, pp. 1-8, 1990.

[2] G. T. A. Kovacs, *Micromachined Transducers Sourcebook*, WCB/McGraw-Hill, 1998.

[3] W. C. Tang, M. G. Lim, and R. T. Howe, "Electrostatically balanced comb drive for controlled levitation," *Tech. Dig., IEEE Solid-State Sensor and Actuator Workshop*, pp. 23, 1990.

[4] V. Kaajakari and A. Lal, "Electrostatic batch assembly of surface MEMS using ultrasonic triboelectricity," *Proc. MEMS'01*, p. 10, 2001.

[5] J. M. Rabaey, *Digital Integrated Circuits*, Prentice Hall, 1996.

[6] http://www.mosis.org

[7] C.-C. Lin, R. Ghodssi, A. A. Ayon, E.-Z. Chen, S. Jacobson, K. Breuer, A. H. Epstein, and M. A. Schmidt, "Fabrication of a micro turbine/bearing rig," *IEEE Solid-State Sensor and Actuator Workshop*, late news poster, 1998.

[8] Z. Liu, M. Kim, V. Narayanan, and E. C. Kan, "Process and device characteristics of self-assembled metal nano-crystal EEPROM," *Superlattices and Microstructures*, pp. 393, Dec. 2000.